Journal of Materials Chemistry C

ROYAL SOCIETY OF CHEMISTRY

PAPER

View Article Online
View Journal

Cite this: DOI: 10.1039/d5tc03319e

Magneto-optical Raman effect of WS_2 tuned by a plasmonic gold nanograting

Yang Yang, †*[a] Yang Guo,†[ab] Ruochen Zhang,[c] Hao Chang,[ad] Cai Luo,[ae] Junjie Li *[ab] and Changzhi Gu*[ab]

Received 5th September 2025,
Accepted 28th October 2025

DOI: 10.1039/d5tc03319e

rsc.li/materials-c

In recent years, the magento-optical properties of two-dimensional transition metal dichalcogenides (TMDCs) have garnered significant attention from scholars, owing to their potential applications in spintronic and valleytronic devices. Hybridizing TMDCs with plasmonic nanostructures has been demonstrated to be an effective route to modulate the optical properties of TMDCs. In this study, the modulation effects of a plasmonic Au nanograting (Au-NG) on the magneto-optical properties of monolayer WS_2 were systematically investigated utilizing polarized-Raman spectroscopy. Raman modes of WS_2 exhibited regular intensity fluctuation with increasing magnetic fields. It is worth noting that the magnetic-field-dependent Raman intensity of WS_2 on Au-NG exhibited obvious differences from WS_2 on Si and Au films, of which the critical magnetic field was 5.5 T in both the parallel and crossed polarization configurations. The critical magnetic field was promoted to 6.5 T when laser polarization was perpendicular to Au-NG. Even more attractively, the critical magnetic field was lowered to 3.5 T when the laser polarization was parallel to Au-NG. This phenomenon can be attributed to the localized surface plasmonic resonance effect from Au-NG, leading to the opposite electric field response under different polarizations. This work not only deepens the understanding of the magento-optical properties of WS_2, but also offers a useful new approach for designing high-sensitivity magneto-optic devices based on WS_2.

1. Introduction

In recent years, the magneto-optical properties of two-dimensional (2D) transition metal dichalcogenides (TMDCs) have gained significant attention from scholars because of their potential applications in magneto-optic devices, such as spintronics, smart sensors, modulators, and quantum computing.[1–3] Various optical techniques, such as photoluminescence (PL), Raman, the magneto-optic Kerr effect (MOKE), and ultrafast spectroscopy, have been carried out to investigate the magneto-optical properties of 2D TMDCs.[4–8] Among these optical techniques, Raman spectroscopy has been recognized as a sensitive method to investigate the magneto-optical properties of nonmagnetic TMDCs.[6,9,10] Polarized-Raman spectroscopy has been demonstrated as an effective method to distinguish the Raman modes and characterize the subtle changes of structural and electronic properties of TMDCs.[11,12] It is predicted that the variations in the magneto-optical properties of TMDCs can be expressed in the changes in Raman spectra under different polarization configurations. By employing polarized-Raman scattering, Ji *et al.* demonstrated a prominent evolution of the intensity of the A_1' mode in MoS_2 with increasing magnetic fields.[6] However, as reported in the literature, the critical magnetic field for the magneto-Raman response of TMDCs is normally higher than 5 T, limiting their practical applications in magneto-optics.

It is well-known that the atomic-scale thickness of TMDCs inherently limits their optical response due to weak light–matter interactions. It has been demonstrated that through hybridizing with plasmonic nanoscale metals, such as noble metallic nanoparticles and nanostructures, the optical properties of 2D TMDCs could be selectively modulated, promising widespread applications in optoelectronic devices, such as photodetectors, photovoltaics and light-emitting devices.[13–15] Among semiconducting TMDCs, monolayer WS_2 holds a direct band gap with a theoretical value of ~2.1 eV,[16,17] high emission quantum yield,[18] and large exciton/trion binding energy,[19,20] large surface area and active sulfur atoms,[21] making it a fascinating candidate for the

[a] Beijing National Laboratory for Condensed Matter Physics, Institute of Physics, Chinese Academy of Sciences, Beijing 100190, China. E-mail: yang.yang@iphy.ac.cn, jjli@iphy.ac.cn, czgu@iphy.ac.cn
[b] School of Physical Sciences, CAS Key Laboratory of Vacuum Physics University of Chinese Academy of Sciences, Beijing 100190, China
[c] Laser Micro/Nano Fabrication Laboratory, School of Mechanical Engineering, Beijing Institute of Technology, Beijing 100081, China
[d] Center on Nanoenergy Research, Guangxi Colleges and Universities Key Laboratory of Blue Energy and Systems Integration, School of Physical Science & Technology, Guangxi University, Nanning 530004, China
[e] Key Laboratory for Microstructural Material Physics of Hebei Province, School of Science, Yanshan University, Qinhuangdao 066004, China
† These authors contributed equally.

applications of electronic, optoelectronic and photocatalysis devices.[22–26] The optical properties of WS_2 have been obviously enhanced through coupling with periodic plasmonic nanostructures.[27–29] The absorption at the band edge of WS_2 was enhanced by 4 times on periodic Ag nanodisk arrays.[30] Shi *et al.* reported a large second-harmonic generation (SHG) enhancement factor of 400 in WS_2 on an Ag nanogroove grating with subwavelength pitch.[31] A photoluminescence (PL) enhancement of 32-fold has been realized from the double WS_2 on nanogroove arrays.[28] Taking advantage of plasmonic nanostructures as a platform for surface-enhanced Raman scattering, the Raman signal of WS_2 can be prominently enhanced. A four-fold enhancement in Raman scattering has been achieved on the hybrid of WS_2 and a periodic Ag nanoprism array.[32] Moreover, owing to the polarization-dependences of the plasmonic resonance effect on periodic metallic nanostructures, the Raman intensity of the TMDCs exhibited significant polarization selection.[33,34] Therefore, hybridizing monolayer WS_2 with periodic nanostructures is predicted to be a new route to improve the sensitivity of magneto-optical Raman responses.

In this work, we systematically studied the plasmonic effect of an Au nanograting (Au-NG) on the magneto-optical properties of monolayer WS_2 utilizing polarized-Raman spectroscopy. The intensity of the Raman spectra of WS_2 exhibited regular fluctuations as the magnetic field increased. Remarkably, the magnetic-field-dependent Raman intensity of WS_2 on Au-NG exhibited obvious differences from that of WS_2 on SiO_2/Si and Au films. The critical magnetic field was promoted to 6.5 T when the laser polarization was perpendicular to Au-NG, whereas the critical magnetic field was pushed down to 3.5 T when the laser polarization was parallel to Au-NG. This significant discrepancy can be attributed to the localized surface plasmonic resonance (LSPR) effect arising from Au-NG, which modulated the electric field density under different polarizations. These results not only provide an unambiguous insight into the magneto-optical properties of WS_2 but also demonstrate that plasmonic nanostructures could effectively lower the critical magnetic field, guaranteeing a new route for the design and application of magneto-optic devices based on TMDCs.

2. Experimental

2.1. Sample preparations

Monolayer WS_2 was mechanically exfoliated from bulk WS_2 single crystals (HQ Graphene) and transferred onto a 100 nm-thick SiO_2/Si substrate, Au film deposited on a Si substrate and a substrate with an Au-NG pattern, separately, using polydimethylsiloxane stamps through a dry-transfer technique.[35] Au-NG was fabricated using E-beam lithography and followed by electron beam deposition techniques.

2.2. Measurements

Room-temperature Raman spectra were collected using a confocal micro-Raman spectrometer (HORIBA HR Evolution). A 532 nm laser was employed as the excitation source, and the laser power was fixed as 0.7 mW in order to prevent the heating effects. Raman mapping was also performed using the same Raman spectrometer. The sample was moved with a step size of 0.5 μm in the mapping measurement. The integration time for each point was set to 1 s. The low-temperature magneto-Raman measurements were performed using a custom built cryo-Raman system by coupling a cryostat-magnet (attoDRY1100) with a spectrometer (HORIBA iHR550) equipped with a liquid nitrogen cooled charge coupled device. The temperature was fixed at 4 K, while the magnetic field was perpendicular to the sample surface and varied from 0 to 9 T with a step of 0.5 T. A linearly polarized 532 nm laser was used as the excitation source of power $\sim$2 mW.

2.3. Simulation

The electric field distribution on Au-NG was simulated using the finite difference time domain (FDTD) method (Lumerical FDTD solutions software package). The simulation region was configured to accommodate changes in the periods. The boundaries of the simulation region were set as a perfectly matched layer (PML) with 8 layers. The amplitude of the 532 nm laser was set to 1. A Gaussian laser source with line polarization was focused on the surface at an angle of 90°. Two different simulation results were achieved by varying the polarization of the illuminated laser source.

3. Results and discussion

Fig. 1(a) presents a schematic illustration of the hybrid nanostructure of WS_2 and Au-NG (WS_2/Au-NG). The geometrical parameters of Au-NG were of a trench width of 200 nm, a periodicity of 500 nm and a depth of 35 nm, respectively, as confirmed by the SEM image shown in Fig. 1(b). Fig. 1(c) exhibits the optical image of the WS_2/Au-NG hybrid nanostructure, in which the location of monolayer WS_2 (1L-WS_2) was labeled. Also, the area of Au-NG was 80 × 80 μm^2, as shown in Fig. 1(c). A region of 19 × 14 μm^2 was selected on the WS_2/Au-NG hybrid for Raman mapping measurement, in which monolayer WS_2 on the Au nanograting and Au film were both enclosed. The Raman mapping image was created using the peak intensity of the 2LA(M) mode of WS_2 (Fig. S1, SI). One can see that the Raman intensity on Au-NG exhibits relatively uniform distribution, indicating that monolayer WS_2 has been well transferred on Au-NG. Moreover, the intensity of the 2LA(M) mode for WS_2/Au-NG is lower than that of WS_2/Au. As depicted in Fig. 1(d), the sample was mounted on the optical stick and inserted into the vacuum chamber of the cryo-magnet for Raman spectra measurements. The magnetic field direction was perpendicular to the sample surface. The geometry setups of the polarized-Raman measurements are illustrated in Fig. 1(e)–(h). The polarization of the incident laser was set to parallel with the *x*-axis of lab coordinates, named H-pol, whereas the incident polarization paralleling to the *y*-axis was named V-pol. The trench direction of Au-NG paralleled the *y*-axis of the lab coordinates. Therefore, the polarization of the incident laser crossed and paralleled the direction of Au-NG in

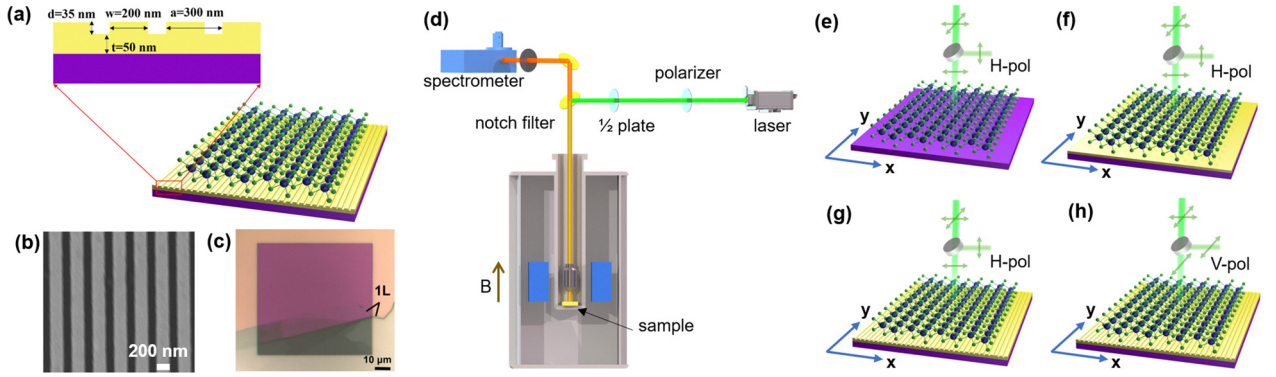

Fig. 1 (a) Schematic illustration, (b) SEM image, and (c) optical microscope image of the WS_2/Au-NG hybrid nanostructure. (d) Schematic illustration of the experimental setup of low-temperature magneto-Raman measurement. (e)–(h) Schematic illustrations of the polarization geometries of Raman measurements on different WS_2 samples.

the H-pol and V-pol setup, respectively. The Raman spectra were collected in two polarization setups, in which the directions of the collection polarization were set to parallel (HH, VV) and perpendicular (HV, VH) to the incident polarization, respectively.

Fig. 2(a) presents the room-temperature polarized-Raman spectra of WS_2 on a SiO_2/Si substrate (WS_2/SiO_2/Si), which exhibit the Raman characteristics of WS_2 reported in the literature.[36–38] The Raman modes located at approximately 350, 358 and 417 cm^{-1} are assigned as the second-order in-plane longitudinal acoustic mode 2LA(M), in-plane optical phonon mode E′ and out-of-plane optical vibrational mode A_1', respectively. Interestingly, the lineshapes of the parallel polarized Raman spectra of the samples on plasmonic substrates (Au film and Au-NG) are similar to those of WS_2/SiO_2/Si, as shown in Fig. 2(b)–(d). Compared with the Raman spectra of WS_2/SiO_2/Si, the intensity of the parallelled Raman spectra of WS_2 on Au film (WS_2/Au) and Au-NG (WS_2/Au-NG) was significantly enhanced by 3.5 and 4.2 times, respectively, under the H-polarized incident excitation, as presented in Fig. 2(b) and (c). A similar enhancement in the Raman spectra of WS_2 has been reported in previous literatures, which was attributed to the LSPR effect from the plasmonic substrates.[32,39] Remarkably, the parallel Raman spectrum of WS_2/Au-NG under the V-polarized incident excitation was not enhanced and even was a little lower than that of WS_2/SiO_2/Si, as shown in Fig. 2(d). On the other hand, in the crossed polarization setup, the intensity of the 2LA(M) and A_1' modes decreased significantly compared with the E′ mode, in Fig. 2(a)–(d). Similar polarization-dependent Raman intensity evolutions have been observed from monolayer MoS_2 on the Au nanograting.[34] The prominent enhanced Raman intensity was attributed to the strongest plasmonic hot spots formed across the slits when excitation polarization was perpendicular to the grating. Therefore, the huge discrepancies in the Raman intensity shown in Fig. 2(c) and (d) can be attributed to the variation of the plasmonic hot spots under different excitation laser directions.[33,40] This prediction can also be confirmed from the PL spectra of WS_2 on different substrates (Fig. S2, SI). The PL intensities of WS_2/Au-NG and WS_2/Au under H-polarization excitation are very close, which are approximately six- and seven-fold those of WS_2/SiO_2/Si. The PL intensity of WS_2/Au did not show obvious polarization dependence. Noteworthily, the PL spectra of WS_2/Au-NG exhibited

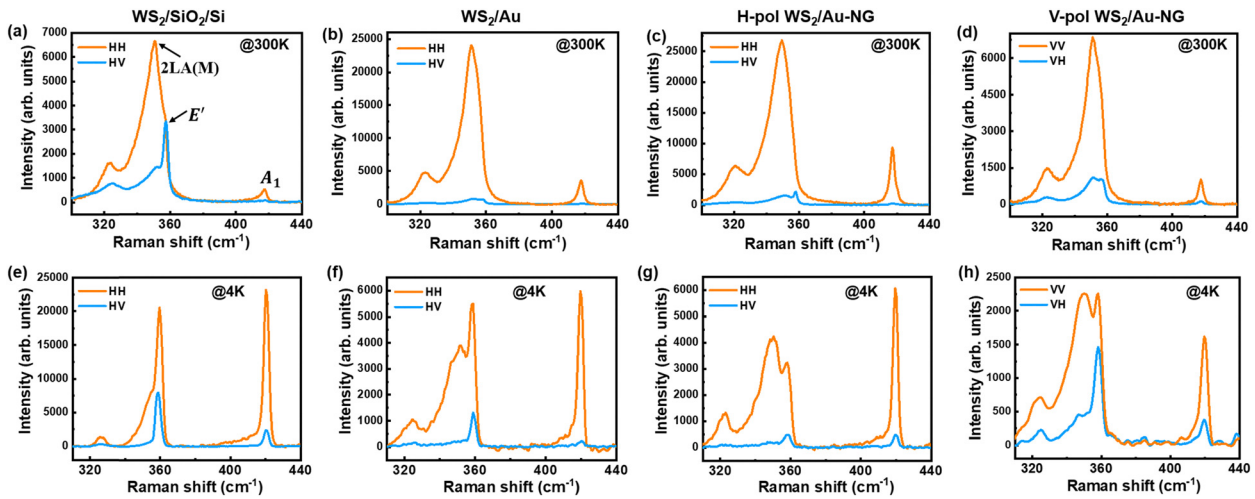

Fig. 2 Polarized-Raman spectra of different WS_2 samples collected at (a)–(d) room temperature and (e)–(h) low temperature (4 K), respectively.

remarkable polarization dependence. The PL intensity under H-polarization excitation is two times higher than that of V-polarization excitation. These results clearly demonstrated that the Au nanograting has prominent polarization-dependent enhancement of the PL emission of monolayer WS_2 owing to the LSPR effect.

Fig. 2(e)–(h) present the polarized-Raman spectra of different WS_2 samples collected at 4 K. It is noteworthy that the parallel spectra for the WS_2 samples are different from each other, in contrast to the RT spectra. The A_1' modes were significantly enhanced in the parallel polarization setup. As shown in Fig. 2(e), the 2LA(M) mode of $WS_2/SiO_2/Si$ shrank significantly in the parallel spectrum, compared with its counterpart at room temperature. The low-temperature parallel spectra of WS_2 on plasmonic substrates exhibited obvious differences from those of $WS_2/SiO_2/Si$, in which the 2LA(M) mode was significantly enhanced and became comparable with the E′ mode, as exhibited in Fig. 2(f)–(h). What is more, the Raman intensity of WS_2/Au-NG is not different too much under VV and VH polarizations, as presented in Fig. 2(h).

Fig. 3 presents the polarized-Raman spectra of different WS_2 samples as a function of magnetic fields. As shown in Fig. 3(a), the intensities of the polarized Raman spectra decrease with increasing field, and reach the lowest value at approximate 5 T, then recover with continuous increasing field. Obviously, the 2LA(M) mode of $WS_2/SiO_2/Si$ exhibited obvious magnetic field induced intensity fluctuation in the parallel polarization setup. On the other hand, the Raman intensity displays an anticorrelated evolution in the crossed polarization setup, as presented in Fig. 3(b). However, the variation of the 2LA(M) mode was not significant in contrast to the E′ and A_1' modes. Similar to $WS_2/SiO_2/Si$, the polarized Raman spectra of WS_2 on the Au film and Au-NG also exhibited regular intensity fluctuation with increased magnetic field, as exhibited in Fig. 3(c)–(h). Noteworthily, the intensity fluctuations of the 2LA(M) mode for WS_2 on the plasmonic substrates are more prominent than those on the SiO_2/Si substrate. In particular, the 2LA(M) mode exhibited prominent variations even at the crossed polarization setup, as illustrated in Fig. 3(d), (f) and (h).

The magnetic field-dependent Raman spectra for these WS_2 samples were deconvoluted using Lorentz/Gaussian-mixed function, in order to get a clear view of the magnetic field dependence of the peak intensity of WS_2 on different substrates. As presented in Fig. 4(a)–(c), the magnetic field dependences of the intensities of the 2LA(M), A_1' and E′ modes for $WS_2/SiO_2/Si$ exhibit similar behaviors. The peak intensities vary oppositely in the VV and VH polarization configurations. The maximum intensity in the VH configuration and the minimum intensity in the VV configuration take place at 5.5 T. The similar magnetic field induced intensity modulations are also observed on WS_2/Au, as displayed in Fig. 4(d)–(f). The critical magnetic field for WS_2/Au is also at 5.5 T, which is a little higher than that for $WS_2/SiO_2/Si$. In addition, one can see that the Raman spectra at 9 T can nearly recover to that of the spectra at 0 T. These results presented in Fig. 4(a)–(f) show good agreement with those in previous reports.[9,41]

It is worth noting that the field dependencies of the WS_2 on Au-NG are much different from those of the WS_2 on the Si wafer and Au film. In particular, the intensity field-dependent behaviors under the crossed polarization setup are abnormal. The critical field was promoted to 6.5 T, and the intensity of the Raman modes did not recover back until 9 T, while the excited laser polarization crossed the nanograting, as illustrated in Fig. 4(g)–(i). In contrast, the critical field was lowered to 3.5 T, while the excited laser polarization paralleled the nanograting, as illustrated in Fig. 4(j)–(l). Moreover, one can see that the intensities of the Raman modes were enhanced and the intensity at 9 T was much higher than that at 0 T. One can see in Fig. 4(g)–(l) that the critical field between the parallel and crossed polarization

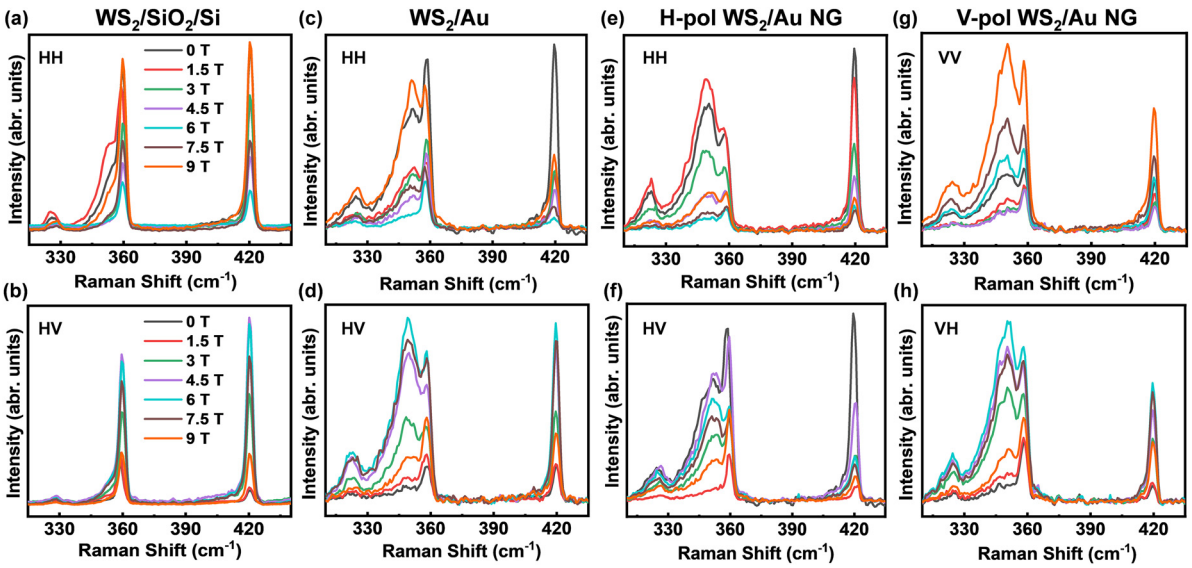

Fig. 3 Magnetic field-dependent Raman spectra of different WS_2 samples in parallel and crossed polarization configurations. Polarized-Raman spectra of (a and b) $WS_2/SiO_2/Si$, (c and d) WS_2/Au. Polarized-Raman spectra of WS_2/Au NG under (e and f) H-polarization and (g and h) V-polarization excitations, separately.

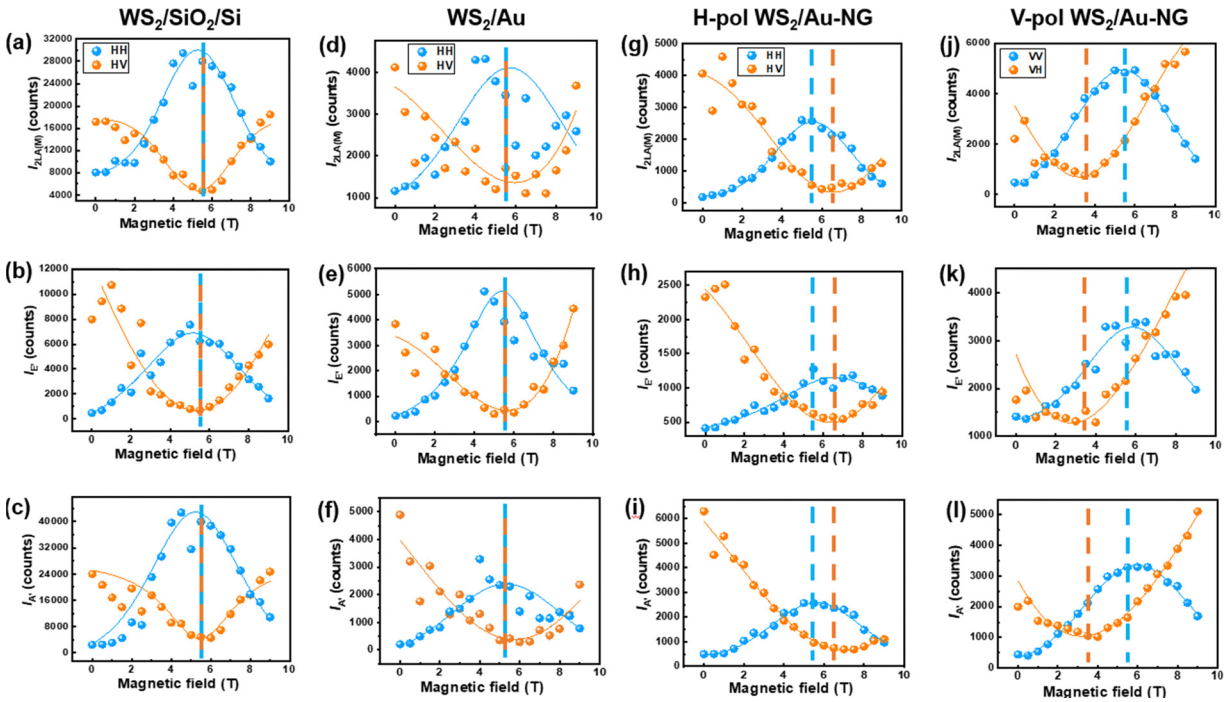

Fig. 4 Magnetic field induced modulation of the Raman intensity under different polarization configurations. Magnetic field dependent polarized-Raman intensity of the 2LA(M), A_1' and E′ modes for (a–c) $WS_2/SiO_2/Si$, (d)–(f) WS_2/Au, (g)–(i) H-pol WS_2/Au-NG, and (j)–(l) V-pol WS_2/Au-NG.

setups is discrepant on the WS_2 on Au-NG. For the incident H-polarization case, there is only a difference of 2 T between the two polarization setups. Remarkably, a discrepancy of 3 T appeared on WS_2 under the V-polarization.

To quantify the effects of magnetic fields on the Raman intensity of WS_2, the magneto-Raman intensity (MRI) of monolayer WS_2 on two different substrates was calculated according to previous literatures,[6,9]

$$\text{Magneto-Raman intensity} = \frac{I(B) - I(0)}{I(0)} \times 100\%$$

determined from the Raman intensity $I(B)$ obtained under different magnetic fields.

As exhibited in Fig. 5(a), the MRIs of the 2LA(M) and A_1' modes are much higher than that of the E′ mode. In contrast, the MRI of the A_1' mode for plasmonic substrates dropped obviously, and became close to that of the E′ mode. The MRI of 2LA(M) was much higher than those of the other two modes, as presented in Fig. 5(c), (e) and (g). This observation shows good agreement with that exhibited in Fig. 2. Although the MRIs of these three modes varied on plasmonic substrates, the critical magnetic field does not change under the parallel polarization

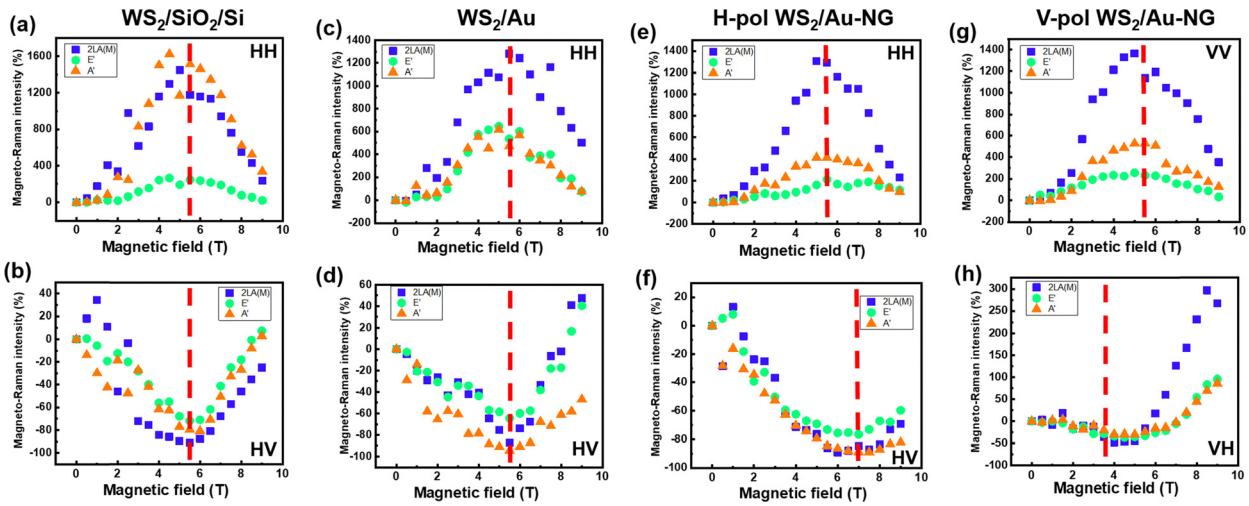

Fig. 5 Polarized magneto-Raman intensity of the 2LA(M), A_1' and E′ modes for (a and b) $WS_2/SiO_2/Si$, (c and d) WS_2/Au, (e and f) H-pol WS_2/Au-NG, and (g and h) V-pol WS_2/Au-NG.

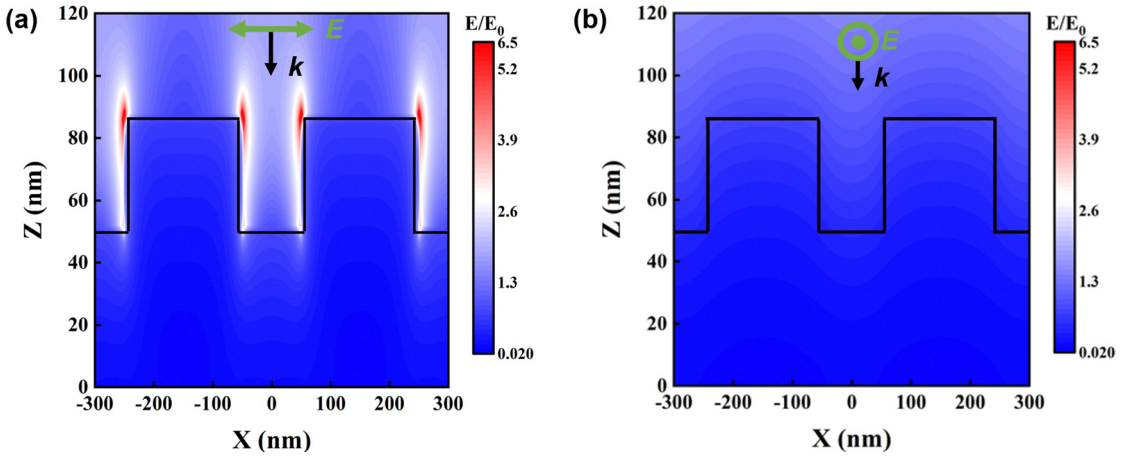

Fig. 6 Cross-section view of the simulated electric field distribution of the Au nanograting under the excitation of a 532 nm laser with (a) horizontal polarization and (b) vertical polarization, respectively.

setup. In the crossed polarization setup, the MRI from WS_2/Au is similar to that of $WS_2/SiO_2/Si$. Moreover, the MRIs can clearly illustrate the plasmonic nanostructure on the magneto-Raman behaviors of WS_2. As shown in Fig. 5(f) and (h), the critical field was promoted to 6.5 T and was lowered to 3.5 T while the incident laser polarization crosses and was parallel to the nanograting, respectively. Remarkably, the lowest MRI for the V-polarization is just approximately 50%, whereas the lowest MRI for the other three samples could be down to 100%. These observations undoubtedly imply that the plasmonic nanostructures effectively modulated the magneto-Raman response of WS_2.

In order to investigate the modulation mechanism of the LSPR effect on the magneto-Raman behaviors of WS_2, optical simulation with the FDTD Maxwell solver method was performed based on the structure details, which have been informed by the SEM image shown in Fig. 1(b). The images of the electric field intensity distribution along the x–z axis of the Au nanograting under excitation by two types of linearly polarized light are shown in Fig. 6(a) and (b). As shown in Fig. 6(a), the electric field was enhanced by 1.5 times as a result of the LSPR. Hot-spots were excited at the edges of the nanograting grooves under the horizontal polarization excitation due to the interaction between the external field with nano-confined free electrons near the structure tip.[42] On the other hand, the electric field under vertical excitation is just $\sim$0.6 compared to that of the incident laser, as illustrated in Fig. 6(b). These simulation results clearly explain the Raman data presented in Fig. 2(c) and (d).

4. Conclusions

In this work, we presented a systematic polarized Raman study of the modulation of the plasmonic Au nanograting on the magneto-optical properties of monolayer WS_2. The magnetic field evolution of the Raman spectra exhibited significant polarization dependences. Moreover, the magnetic-field-dependent Raman intensity of WS_2 on the Au nanograting exhibited obvious differences for WS_2 on the Si and Au films. For WS_2 on the Si and Au films, the critical magnetic field was at 5.5 T in both the parallel and crossed polarization configurations. In sharp contrast, the critical magnetic field was promoted to 6.5 T when laser polarization was perpendicular to the nanograting. Remarkably, the critical magnetic field was lowered to 3.5 T when laser polarization was parallel to the nanograting, which could be attributed to the suppressed electric field response due to the LSPR effect from the Au nanograting. These results not only deepen our understanding on the magento-optical properties of WS_2, but also pave a new route for fabricating optoelectronic devices based on WS_2.

Author contributions

Yang Yang: conceptualization, methodology, writing, project administration, and funding acquisition. Yang Guo: methodology, funding acquisition, and resources. Ruochen Zhang: data curation and visualization. Hao Chang: data curation. Cai Luo: resources. Junjie Li: funding acquisition and supervision. Changzhi Gu: funding acquisition and supervision.

Conflicts of interest

There are no conflicts to declare.

Data availability

The data supporting this article have been included in the supplementary information (SI). Supplementary information: Raman mapping image of monolayer WS_2 on Au nanograting, PL spectra of monolayer WS_2 on different substrates, low temperature magneto-Raman spectra of monolayer WS_2 on different substrates. See DOI: **https://doi.org/10.1039/d5tc03319e**.

Acknowledgements

This work was supported by the National Natural Science Foundation of China (Grant No. 62175253), the National Key Research and Development Program of China (Grant No. 2024YFA1207700, 2023YFF0715902, and 2022YFA1204100), National Natural Science Foundation of China (Grant No. 62174179, 12074420, and U21A20140), CAS Project for Young Scientists in Basic Research (Grant No. YSBR-056), and the Strategic Priority Research Program of CAS (Grant No. XDB0670100 and XDB33020200).

References

1 Y. Khan, S. M. Obaidulla, M. R. Habib, A. Gayen, T. Liang, X. Wang and M. Xu, Recent breakthroughs in two-dimensional van der Waals magnetic materials and emerging applications, *Nano Today*, 2020, **34**, 100902.

2 A. Arora, Magneto-optics of layered two-dimensional semiconductors and heterostructures: Progress and prospects, *J. Appl. Phys.*, 2021, **129**(12), 120902.

3 Q. H. Wang, A. Bedoya-Pinto, M. Blei, A. H. Dismukes, A. Hamo, S. Jenkins, M. Koperski, Y. Liu, Q.-C. Sun, E. J. Telford, H. H. Kim, M. Augustin, U. Vool, J.-X. Yin, L. H. Li, A. Falin, C. R. Dean, F. Casanova, R. F. L. Evans, M. Chshiev, A. Mishchenko, C. Petrovic, R. He, L. Zhao, A. W. Tsen, B. D. Gerardot, M. Brotons-Gisbert, Z. Guguchia, X. Roy, S. Tongay, Z. Wang, M. Z. Hasan, J. Wrachtrup, A. Yacoby, A. Fert, S. Parkin, K. S. Novoselov, P. Dai, L. Balicas and E. J. G. Santos, The Magnetic Genome of Two-Dimensional van der Waals Materials, *ACS Nano*, 2022, **16**(5), 6960–7079.

4 S. Du, F. Jin, X. Liu, X. Huang, Y. Yang, H. Yang, J. Li, Q. Zhang, S. Meng, Y. Guo and C. Gu, Brightening and Control of Spin-Forbidden Dark Excitons in a Strained Monolayer Semiconductor, *Laser Photonics Rev.*, 2023, **17**(10), 2300185.

5 C. Serati de Brito, B. L. T. Rosa, A. Chaves, C. Cavalini, C. R. Rabahi, D. F. Franco, M. Nalin, I. D. Barcelos, S. Reitzenstein and Y. G. Gobato, Probing the Nature of Single-Photon Emitters in a WSe_2 Monolayer by Magneto-Photoluminescence Spectroscopy, *Nano Lett.*, 2024, **24**(42), 13300–13306.

6 J. Ji, A. Zhang, J. Fan, Y. Li, X. Wang, J. Zhang, E. W. Plummer and Q. Zhang, Giant magneto-optical Raman effect in a layered transition metal compound, *Proc. Natl. Acad. Sci. U. S. A.*, 2016, **113**(9), 2349–2353.

7 J. C. Sell, J. R. Vannucci, D. G. Suárez-Forero, B. Cao, D. W. Session, H. J. Chuang, K. M. McCreary, M. R. Rosenberger, B. T. Jonker, S. Mittal and M. Hafezi, Magneto-optical measurements of the negatively charged 2s exciton in WSe_2, *Phys. Rev. B*, 2022, **106**(8), L081409.

8 E. J. McCormick, M. J. Newburger, Y. K. Luo, K. M. McCreary, S. Singh, I. B. Martin, E. J. Cichewicz, B. T. Jonker and R. K. Kawakami, Imaging spin dynamics in monolayer WS_2 by time-resolved Kerr rotation microscopy, *2D Mater.*, 2018, **5**(1), 011010.

9 L. Du, Z. Jia, Q. Zhang, A. Zhang, T. Zhang, R. He, R. Yang, D. Shi, Y. Yao, J. Xiang, G. Zhang and Q. Zhang, Electronic structure-dependent magneto-optical Raman effect in atomically thin WS_2, *2D Mater.*, 2018, **5**(3), 035028.

10 Y. Yang, W. Liu, Z. Lin, K. Zhu, S. Tian, Y. Huang, C. Gu and J. Li, Micro-Defects in Monolayer MoS_2 Studied by Low-Temperature Magneto-Raman Mapping, The, *J. Phys. Chem. C*, 2020, **124**(31), 17418–17422.

11 R. Saito, Y. Tatsumi, S. Huang, X. Ling and M. S. Dresselhaus, Raman spectroscopy of transition metal dichalcogenides, *J. Phys.: Condens. Matter*, 2016, **28**(35), 353002.

12 S. Zhang, N. Zhang, Y. Zhao, T. Cheng, X. Li, R. Feng, H. Xu, Z. Liu, J. Zhang and L. Tong, Spotting the differences in two-dimensional materials - the Raman scattering perspective, *Chem. Soc. Rev.*, 2018, **47**(9), 3217–3240.

13 M. Cotrufo, L. Sun, J. Choi, A. Alù and X. Li, Enhancing functionalities of atomically thin semiconductors with plasmonic nanostructures, *Nanophotonics*, 2019, **8**(4), 577–598.

14 P. Sriram, A. Manikandan, F.-C. Chuang and Y.-L. Chueh, Hybridizing Plasmonic Materials with 2D-Transition Metal Dichalcogenides toward Functional Applications, *Small*, 2020, **16**(15), 1904271.

15 Y. Yang, W. G. liu, Z. T. Lin, R. H. Pan, C. Z. Gu and J. J. Li, Plasmonic hybrids of two-dimensional transition metal dichalcogenides and nanoscale metals: Architectures, enhanced optical properties and devices, *Mater. Today Phys.*, 2021, **17**, 100343.

16 W. Zhao, Z. Ghorannevis, L. Chu, M. Toh, C. Kloc, P.-H. Tan and G. Eda, Evolution of Electronic Structure in Atomically Thin Sheets of WS_2 and WSe_2, *ACS Nano*, 2013, **7**(1), 791–797.

17 A. Kuc, N. Zibouche and T. Heine, Influence of quantum confinement on the electronic structure of the transition metal sulfide TS_2, *Phys. Rev. B: Condens. Matter Mater. Phys.*, 2011, **83**(24), 245213.

18 L. Yuan and L. Huang, Exciton dynamics and annihilation in WS_2 2D semiconductors, *Nanoscale*, 2015, **7**(16), 7402–7408.

19 Z. Ye, T. Cao, K. O'Brien, H. Zhu, X. Yin, Y. Wang, S. G. Louie and X. Zhang, Probing excitonic dark states in single-layer tungsten disulphide, *Nature*, 2014, **513**(7517), 214–218.

20 N. Peimyoo, J. Shang, C. Cong, X. Shen, X. Wu, E. K. L. Yeow and T. Yu, Nonblinking, Intense Two-Dimensional Light Emitter: Monolayer WS_2 Triangles, *ACS Nano*, 2013, **7**(12), 10985–10994.

21 X. Tang, Q. Hao, X. Hou, L. Lan, M. Li, L. Yao, X. Zhao, Z. Ni, X. Fan and T. Qiu, Exploring and Engineering 2D Transition Metal Dichalcogenides toward Ultimate SERS Performance, *Adv. Mater.*, 2024, **36**(19), 2312348.

22 N. Peimyoo, W. Yang, J. Shang, X. Shen, Y. Wang and T. Yu, Chemically Driven Tunable Light Emission of Charged and Neutral Excitons in Monolayer WS_2, *ACS Nano*, 2014, **8**(11), 11320–11329.

23 W. Yin, X. Bai, P. Chen, X. Zhang, L. Su, C. Ji, H. Gao, H. Song and W. W. Yu, Rational Control of Size and Photoluminescence of WS_2 Quantum Dots for White Light-Emitting Diodes, *ACS Appl. Mater. Interfaces*, 2018, **10**(50), 43824–43830.

24 T. Georgiou, R. Jalil, B. D. Belle, L. Britnell, R. V. Gorbachev, S. V. Morozov, Y.-J. Kim, A. Gholinia, S. J. Haigh, O. Makarovsky, L. Eaves, L. A. Ponomarenko, A. K. Geim, K. S. Novoselov and A. Mishchenko, Vertical field-effect transistor based on graphene–WS_2 heterostructures for flexible and transparent electronics, *Nat. Nanotechnol.*, 2013, **8**(2), 100–103.

25 J. Singh, R. Sebait, P. Raj Adhikari, D. Dridi, N.-N. Khushboo, R. Vu, P. Soni and P. Nguyen-Tri, WS2 Nanosheets Modified with Ag Nanoparticles as Visible-Light Photocatalysis for Hot-Electron-Mediated Plasmonic Charge Transfer in the Degradation of Textile and Pharmaceutical Waste, *ACS Appl. Nano Mater.*, 2025, **8**(29), 14607–14621.

26 J. Singh, R. K. Soni, D. D. Nguyen, V. Kumar Gupta and P. Nguyen-Tri, Enhanced photocatalytic and SERS performance of Ag nanoparticles functionalized MoS_2 nanoflakes, *Chemosphere*, 2023, **339**, 139735.

27 S. Liu, F. Deng, W. Zhuang, X. He, H. Huang, J.-D. Chen, H. Pang and S. Lan, Optical Introduction and Manipulation of Plasmon–Exciton–Trion Coupling in a Si/WS_2/Au Nanocavity, *ACS Nano*, 2022, **16**(9), 14390–14401.

28 X. Huang, Y. Guo, S. Du, Q. Bai, C. Sun, L. Hu, R. Zheng, P. Fu, Y. Yang, A. Jin, K. Watanabe, T. Taniguchi, J. Li, B. Liu and C. Gu, Strong Linearly Polarized Emission from Monolayer WS_2 Coupled with Plasmonic Nanocavity Array, *Adv. Opt. Mater.*, 2022, **10**(19), 2200535.

29 Y. Zhang, H.-J. Schill, S. Irsen and S. Linden, Strong coupling between WS_2 monolayer excitons and a hybrid plasmon polariton at room temperature, *Nanophotonics*, 2024, **13**(15), 2847–2856.

30 S. Butun, E. Palacios, J. D. Cain, Z. Liu, V. P. Dravid and K. Aydin, Quantifying Plasmon-Enhanced Light Absorption in Monolayer WS2 Films, *ACS Appl. Mater. Interfaces*, 2017, **9**(17), 15044–15051.

31 J. Shi, W.-Y. Liang, S. S. Raja, Y. Sang, X.-Q. Zhang, C.-A. Chen, Y. Wang, X. Yang, Y.-H. Lee, H. Ahn and S. Gwo, Plasmonic Enhancement and Manipulation of Optical Nonlinearity in Monolayer Tungsten Disulfide, *Laser & Photonics Rev.*, 2018, **12**(10), 1800188.

32 W. Yang, H. Li, J. Chen, J. Yin, J. Li, Y. Wu, B. Mo, T. Wu, B. Sun, Z. Wu, H. Wang, L. Dong and G. Wang, Plasmon-enhanced exciton emissions and Raman scattering of CVD-grown monolayer WS_2 on Ag nanoprism arrays, *Appl. Surf. Sci.*, 2020, **504**, 144252.

33 Q. Hao, J. Pang, Y. Zhang, J. Wang, L. Ma and O. G. Schmidt, Boosting the Photoluminescence of Monolayer MoS_2 on High-Density Nanodimer Arrays with Sub-10 nm Gap, *Adv. Opt. Mater.*, 2018, **6**(2), 1700984.

34 M. F. S. Lemes, A. C. S. Pimenta, G. Lozano Calderón, M. A. Pereira-da-Silva, A. Ames, M. D. Teodoro, G. Migliato Marega, R. Chiesa, Z. Wang, A. Kis and E. Marega Junior, Polarization-Dependent Plasmon-Induced Doping and Strain Effects in MoS_2 Monolayers on Gold Nanostructures, *ACS Nano*, 2025, **19**(2), 2518–2528.

35 P. J. Zomer, M. H. D. Guimarães, J. C. Brant, N. Tombros and B. J. van Wees, Fast pick up technique for high quality heterostructures of bilayer graphene and hexagonal boron nitride, *Appl. Phys. Lett.*, 2014, **105**(1), 013101.

36 H. Zeng, G.-B. Liu, J. Dai, Y. Yan, B. Zhu, R. He, L. Xie, S. Xu, X. Chen, W. Yao and X. Cui, Optical signature of symmetry variations and spin-valley coupling in atomically thin tungsten dichalcogenides, *Sci. Rep.*, 2013, **3**(1), 1608.

37 A. A. Mitioglu, P. Plochocka, G. Deligeorgis, S. Anghel, L. Kulyuk and D. K. Maude, Second-order resonant Raman scattering in single-layer tungsten disulfide WS_2, *Phys. Rev. B: Condens. Matter Mater. Phys.*, 2014, **89**(24), 245442.

38 X. Huang, Y. Gao, T. Yang, W. Ren, H.-M. Cheng and T. Lai, Quantitative Analysis of Temperature Dependence of Raman shift of monolayer WS2, *Sci. Rep.*, 2016, **6**(1), 32236.

39 T. S. Bhattacharya, S. Mitra, S. S. Singha, P. K. Mondal and A. Singha, Tailoring light-matter interaction in WS_2-gold nanoparticles hybrid systems, *Phys. Rev. B*, 2019, **100**(23), 235438.

40 H. Chen, J. Yang, E. Rusak, J. Straubel, R. Guo, Y. W. Myint, J. Pei, M. Decker, I. Staude, C. Rockstuhl, Y. Lu, Y. S. Kivshar and D. Neshev, Manipulation of photoluminescence of two-dimensional $MoSe_2$ by gold nanoantennas, *Sci. Rep.*, 2016, **6**, 22296.

41 W. Liu, Z. Lin, S. Tian, Y. Huang, H. Xue, K. Zhu, C. Gu, Y. Yang and J. Li, Plasmonic Effect on the Magneto-Optical Property of Monolayer WS_2 Studied by Polarized-Raman Spectroscopy, *Appl. Sci.*, 2021, **11**(4), 1599.

42 C. Luo, W. Li, J. Li, Z. Fu, N. Hu, Z. Yu, W. Chang, P. Li, X. Huang, B. Liu, Y. Yang, A. Jin, B. Quan, S. Tian, H. Yang, Y. Guo and C. Gu, Room-Temperature Exciton Polaritons in Monolayer WS_2 Enabled by Plasmonic Bound States in the Continuum, *Nano Lett.*, 2025, **25**(11), 4361–4368.

